# Vanadium promoted molybdenum phosphate catalysts for the vapour phase partial oxidation of methanol to formaldehyde

**Gareth T. Whiting, Jonathan K. Bartley, Nicholas F. Dummer, Graham J. Hutchings and Stuart H. Taylor***

*Cardiff Catalysis Institute, Cardiff University, School of Chemistry, Main Building, Park Place, Cardiff, CF10 3AT, UK.*

*Corresponding author: taylorsh@Cardiff.ac.uk

**Keywords:** Selective oxidation; Methanol; Formaldehyde; Molybdenum phosphate; vanadium phosphate

**Abstract**

The catalytic properties of $(MoO_2)_2P_2O_7$ promoted with vanadium have been investigated for the partial oxidation of methanol, and structure-activity relationships probed using a range of characterization techniques. All unpromoted and promoted molybdenum phosphate catalysts were active, with higher vanadium content achieving both high activity and high formaldehyde selectivity at reaction temperatures around 400 °C. The association between increasing vanadium content and the enhanced activity towards methanol oxidation was attributed to the formation of mixed phase catalysts, in particular $VOHPO_4 \cdot 0.5H_2O/VOPO_4 \cdot 2H_2O$ with $(MoO_2)_2P_2O_7$. The dispersion of vanadium phosphate phases on the surface of $(MoO_2)_2P_2O_7$ was found to substantially enhance the catalytic properties of the molybdenum phosphate catalyst. The data from this study indicate that molybdenum phosphate based catalysts are promising candidates for selective oxidation, and hence worthy of further investigation.

## 1. Introduction

Formaldehyde is an important intermediate in the chemical industry, as it is used in the production of thermosetting resins, antiseptics, and adhesives. It is also essential for the manufacture of a range of other materials such as plywood, carpeting, paper and fertilizers amongst others [1]. Presently there are two competing industrial processes to produce formaldehyde from the oxidation of methanol, which are based on silver and ferric molybdate catalysts [1-5]. The silver process uses a methanol-rich feed (around 40 %) and reaction temperatures around 650 °C, whereas the ferric molybdate process uses a methanol-lean feed (around 8 %), and reaction temperatures in the region of 300 °C [6,7].

Both catalysts produce a high yield of formaldehyde, and the choice of process is determined by the operating and capital costs, as well as product end use, plant size and type of operation [5,8,9]. Over the last decade, the ferric molybdate-catalysed process has dominated the market as a consequence of the higher formaldehyde selectivity.

This paper reports for the first time, the use of molybdenum phosphate catalysts for methanol oxidation to formaldehyde. Molybdenum phosphate materials (MoPO) have received increasing interest in the last decade for use as new cathode materials for lithium and sodium batteries [10]. For catalysis, they are mainly reported for use in the partial propane oxidation reaction, where they are usually promoted by metals such as silver or cerium, and they produce high selectivity to propene at relatively low conversion [11-15]. In general, MoPO phases are usually comprised of $(PO_4)^{3-}$ tetrahedra linked mostly with $(MoO_6)^{6-}$ octahedra [16]. One of the main characteristics of these phosphate materials is their ability to stabilize molybdenum in various oxidation states, *i.e.* $Mo^{6+}$, $Mo^{5+}$, $Mo^{3+}$ and even mixed valencies such as $Mo^{5+}/Mo^{6+}$. These redox properties make them ideal catalysts for oxidation reactions, such as the partial oxidation of propane, and potentially for the partial oxidation of methanol. Transition metal phosphate catalysts have been reported in the literature to be active for numerous partial oxidation reactions, *e.g.* vanadyl pyrophosphate for butane oxidation to maleic anhydride [17,18], and iron phosphate for the oxidative dehydrogenation of isobutyric acid into methacrylic acid [19,20]. There is some evidence to suggest that the role of phosphate tetrahedra is to enhance the redox properties of the catalyst, possibly due to the increase in mobility of the lattice oxygen through the bulk to the surface, where it can re-oxidise the reduced surface during the reaction [21]. Hence, considering the high selectivity to formaldehyde using molybdenum oxide based catalysts, and considering the possible improvement as an

oxidation catalyst by incorporating phosphate groups, the investigation of molybdenum phosphates as catalysts for methanol oxidation is an interesting concept.

Against this background we have started to investigate the efficacy of molybdenum phosphate catalysts for the selective oxidation of methanol to formaldehyde. The effect of adding vanadium into the molybdenum phosphate structure has also been investigated and the affect on catalyst performance evaluated. Catalysts have been prepared using a relatively simple co-precipitation technique, and physico-chemical properties have been studied using a range of characterisation techniques. Catalytic activity for selective methanol oxidation is reported for the first time with these catalyst formulations, and performance is related to the structure of the catalysts.

## 2. Experimental

### *2.1 Catalyst Preparation*

#### *2.1.1 Unpromoted molybdenum phosphates*

The precursor $MoO_2 \cdot HPO_4 \cdot H_2O$ was obtained by dissolving $MoO_3$ (15 g, Sigma- Aldrich, >99.5 %) in $H_3PO_4$ (45 ml, Aldrich, 85 % in $H_2O$, 99.99 %) at 180 °C. Upon cooling of the viscous solution, concentrated $HNO_3$ was added (300 ml, Fisher Chemical, 70 % Analytical grade) and the mixture refluxed for 16 h. After completion of the reaction, the solid phase was recovered by filtration and washed with water and acetone, before drying overnight at 110 °C in air. $MoO_2 \cdot HPO_4 \cdot H_2O$ was calcined (650 °C, 6 h, ramp rate 20 °C $min^{-1}$) to form $(MoO_2)_2P_2O_7$. The nomenclature for the unpromoted precursor is Mo-HPO, and for the unpromoted $(MoO_2)_2P_2O_7$ catalyst, MoPO.

Vanadium promoted molybdenum phosphate catalysts were prepared by adding the desired amount of $V_2O_5$ (Sigma-Aldrich, >98 %) during the phosphation step of the precursor synthesis, where $MoO_3$ and $V_2O_5$ were dissolved in $H_3PO_4$, prior to refluxing with $HNO_3$.

The same procedure was then followed as for the unpromoted precursor and MoPO preparation. The nomenclature of V promoted $(MoO_2)_2P_2O_7$ is MoPO-V*x*, where *x* denotes either 1, 5, 10 or 20 mol % V, in relation to the molar quantity of Mo.

*2.2 Catalyst Characterisation*

Catalyst surface areas were analysed using a Micromeretics Gemini 2360 analyser and were determined by multi-point nitrogen adsorption at -196 °C, prior to data analysis in accordance with the BET method. All catalysts were degassed under a helium atmosphere (120 °C, 2 h) before analysis. Powder X-ray diffraction was used to identify the crystalline phases present in the catalysts. XRD patterns were collected using a PANalytical XPert diffractometer, with a graphite monochromator and a Cu X-ray source operated at 40 kV and 40 mA. Phases were identified by matching the experimental patterns to the ICCD PDF database. Raman spectroscopy was carried out using a Renishaw inVia Raman microscope equipped with a 514 nm laser (argon ion) with an average laser power of 25 mW. Before acquisition of catalyst spectra the system was calibrated using a silicon reference sample. Catalyst samples were flattened onto an aluminium plate before being analysed.

Scanning electron microscopy (SEM) was conducted using a Carl Zeiss EVO 40 microscope, with each sample dispersed on an adhesive carbon disc. Temperature programmed reduction (TPR) experiments were performed using a Quantachrome ChemBET chemisorption analyzer equipped with a TCD detector. Samples were pre-treated in an argon atmosphere at 120 °C for 1 h, prior to analysis under a reducing atmosphere of 10% $H_2$ in Ar, with a flow rate of 50 ml $min^{-1}$. The temperature ranged from room temperature to 750 °C, at a specific ramp rate. XPS analysis was performed using a Kratos Axis Ultra DLD photoelectron spectrometer, equipped with an aluminium monochromatic source and a dual Al/Mg achromatic source. Spectra were acquired over an area of 700 x 300 μm at a pass energy of

40 eV for high resolution scans. All spectra were calibrated to the C(1s) line of adventitious carbon at a binding energy of 284.7 eV.

*2.3 Methanol oxidation*

Catalytic activity for partial gas phase methanol oxidation, was performed in a fixed bed microreactor. 0.3 g of catalyst was held between plugs of quartz wool in the centre of a 5 mm *i.d.* quartz tube, which was placed vertically into a Carbolite tube furnace, with the outlet line heated to prevent condensation of products such as formaldehyde. Mass flow controllers were used to supply the reactant feed mixture of MeOH:$O_2$:He with a molar ratio of 5:10:85, and a total flow rate of 60 ml $min^{-1}$ (GHSV = 12000 $h^{-1}$). To achieve 5 mol. % methanol, helium was passed through a saturator containing liquid methanol (Aldrich, 99.5 %) which was maintained at 8 °C using a thermostatically controlled water bath. The reactor temperature was varied from 25 to 500 °C in incremental steps, at each interval the catalyst was allowed to attain steady state operation before data were collected. Product analysis was carried out using a Varian Star 3400$C_x$ on-line gas chromatograph, which used two columns in a series/bypass configuration to provide separation of all reactants and products (calibrated using gas reference standards). A Carbosieve S-11 (3 m) column was used for the analysis of $O_2$ and CO, accompanied by a Porapak Q (1 m) column to separate methanol (MeOH), dimethyl ether (DME), methyl formate (MF), formaldehyde (FA) and $CO_2$. A TCD was used in series with an FID for product identification and quantification. Methanol conversion in an empty reactor tube reached around 1% at 500 $^oC$.

## 3. Results and Discussion

*3.1 Catalyst Characterisation*

The diffraction patterns of both Mo-HPO and MoPO are shown in Figure 1. The pattern of the highly crystalline Mo-HPO material was observed, and corresponds well with that of the monoclinic structure reported by Kierkegaard [22]. The structure consists of parallel chains, where each chain of $PO_4$ tetrahedra binding together $MoO_6$, are linked by hydrogen atoms. The calcination of the Mo-HPO precursor produced a crystalline orthorhombic $(MoO_2)_2P_2O_7$ phase, (Figure 1b). In contrast to the parallel chains of the precursor, MoPO forms *zig-zagged* chains built up of $MoO_6$ octahedra, where each octahedron shares two Mo-O vertices with other $MoO_6$ octahedra. The remaining three out of four vertices are shared with $PO_4$ tetrahedra, which link together to form $P_2O_7$ groups [23,24].

The Raman spectra for both Mo-HPO and MoPO are shown in Figure 2. As presented, the main bands associated with Mo-HPO are at 962 and 885 $cm^{-1}$, and these are assigned to $(PO_4)^{3-}_{sym}$ stretching mode and (Mo-O-Mo) stretching respectively [25]. Bands at both 1142 and 1079 $cm^{-1}$ can be related to the $(PO_4)^{3-}_{asym}$ bonds, and a weak Raman band displayed at 1001 $cm^{-1}$ is associated with Mo=O stretching. The main band present at 824 $cm^{-1}$ in the spectrum of MoPO (Figure 2b), is that of $(Mo\text{-}O\text{-}Mo)_{asym}$ stretching. A weak band present at 725 $cm^{-1}$ is associated with $P\text{-}O\text{-}P_{sym}$ mode. Further weak bands observed at 860 and 1016 $cm^{-1}$ are assigned to symmetric and asymmetric Mo=O modes respectively, with those observed at 974 and 1154 $cm^{-1}$ assigned to symmetric and asymmetric $(PO_4)^{3-}$ stretching respectively [25]. The Raman spectra were consistent with the phases identified by XRD.

Table 1 shows the BET surface areas of both Mo-HPO and MoPO, both had low surface areas of 1 $m^2\ g^{-1}$. To observe the morphology of each material SEM analysis was performed, and typical images are presented in Figure 3. The morphology of both Mo-HPO and MoPO is very similar, and can be likened to the transformation of $VOHPO_4 \cdot 0.5H_2O$ to $(VO)_2P_2O_7$, whereby the morphology of the parent precursor is unchanged when forming the active catalyst [26]. The precursor Mo-HPO has a rod-like morphology with jagged edges (Figure

3a), whilst after calcination to produce MoPO more slightly rounded and more well-defined rods were formed (Figure 3b).

To investigate the bulk redox behaviour of both materials, TPR analysis was performed, and results are presented in Figure 4. The reduction process for Mo-HPO is initiated at 380 °C, preceded by a further slow increase up to a maximum at 557 °C, with an overall hydrogen consumption of 1421.5 μmol/g. The reduction of $Mo^{6+}$ to $Mo^{4+}$ is a two step process [27], as can be observed by the two peaks at 557 and 579 °C, corresponding to the reduction of $Mo^{6+}$ to $Mo^{5+}$ and $Mo^{4+}$ respectively. The onset temperature of the reduction process of MoPO is initiated at a higher temperature of around 450 °C, with a sharp increase in hydrogen consumption (1646.0 μmol/g), to a maximum at 579 °C.

The diffraction patterns of MoPO promoted with vanadium are shown in Figures 1c-f. Each of the materials analysed are highly crystalline, with the main phase corresponding to orthorhombic $(MoO_2)_2P_2O_7$. The XRD pattern of MoPO-V1 presents no indication that vanadium ions were incorporated into the MoPO structure, as the diffraction pattern was identical to the $(MoO_2)_2P_2O_7$ phase without vanadium added. It is possible that vanadium could be present as an amorphous phase, or as a highly dispersed separate crystalline phase. The addition of a higher quantity of vanadium (MoPO-V5) resulted in additional reflections, visible at 15.5 °, 19.6 ° and 30.4 ° 2θ. These are attributed to the lattice planes (001), (101) and (130) respectively of a $VOHPO_4 \cdot 0.5H_2O$ phase [28-30]. A further increase in vanadium loading (MoPO-V10) not only led to the formation of reflections assigned to $(MoO_2)_2P_2O_7$ and $VOHPO_4 \cdot 0.5H_2O$ phases, but additional reflections at 11.9 ° and 28.7 ° 2θ are attributed to the respective (001) and (101) planes of $VOPO_4 \cdot 2H_2O$ [31]. High concentrations of vanadium (MoPO-V20) led to the disappearance of reflections associated with the $VOHPO_4 \cdot 0.5H_2O$ phase, and reflections only assigned to $VOPO_4 \cdot 2H_2O$ and the main phase $(MoO_2)_2P_2O_7$ were present. The clear formation of separate crystalline vanadium phosphate

phases confirm that solid solutions are not formed during catalyst synthesis, instead the formation of biphasic catalysts are favoured.

The Raman spectra of MoPO and promoted MoPO-V*x* samples are shown in Figures 2c-f. The analysis of MoPO-V1 provided no evidence of vanadium species present, with the only bands present attributed to the main phase, MoPO. MoPO-V5 and MoPO-V10 both have very similar and complex spectra (Figures 2d and 2e), where some bands associated with MoPO are no longer present. However in both cases, there is an extra band assigned to P-O stretching (981 $cm^{-1}$) in the $VOHPO_4.0.5H2O$ phase. This band is dominant in $VOHPO_4.0.5H2O$ and is characteristically higher in frequency than in $(VO)_2P_2O_7$ [32]. The bonding of V=O to structural water in $VOHPO_4 \cdot 0.5H_2O$ increases the polarizability of the bond [31], which gives rise to V-O-P bands at 1109 and 1154 $cm^{-1}$. Although these can not be observed clearly in the spectra, the band at 1154 $cm^{-1}$ assigned to $(PO_4)^{3-}{}_{asym}$ stretching in the MoPO phase [25], is no longer present, but a broad low intensity band is evident between 1120 and 1155 $cm^{-1}$. The spectra of MoPO-V20 (Figure 2f) presents bands, which are not only related to the main $(MoO_2)_2P_2O_7$ phase, but also to those of $VOPO_4.2H_2O$, consistent with results observed in XRD (Figure 1f). The introduction of a band at 1035 $cm^{-1}$ (V-O-P stretching mode) accompanied by a broad band at 925 $cm^{-1}$ (assigned to $(PO_4)^{3-}{}_{sym}$, and it is shifted from 940 $cm^{-1}$), is characteristic of the $VOPO_4.2H_2O$ phase [33]. As in the spectra of both MoPO-V5 and MoPO-V10, the band observed at 1154 $cm^{-1}$ is assigned to V=O, which occurs due to the isolated vanadyl octahedra sharing an equatorial oxygen with a $PO_4$ tetrahedra and forms V=O···V=O chains in a perpendicular direction [32]. The appearance of coupled V-O and P-O bending modes in the $VOPO_4 \cdot 2H_2O$ can also be observed at 574 and 533 $cm^{-1}$ respectively.

The BET surface areas of the V promoted MoPO materials are shown in Table 1. As seen previously for the unpromoted $(MoO_2)_2P_2O_7$, the surface areas are all very low (1-3 $m^2\ g^{-1}$),

although there is a trend where increasing V content slightly increases the surface area. The morphology of V promoted MoPO materials were studied by SEM (Figures 3c-f). Possibly due to the low quantity of V content in both MoPO-V1 and MoPO-V5, the rod shaped morphology of $(MoO_2)_2P_2O_7$ was maintained, with no characteristic VPO morphology present. This finding, accompanied by the absence of reflections and bands in both XRD and Raman spectroscopy, respectively, related to vanadium phosphate (for MoPO-V1), suggests it is highly dispersed. The increased content of 10 and 20 mol % V to MoPO visually confirms the presence of separate VPO phases to that of $(MoO_2)_2P_2O_7$ (Figures 3e and 3f), as the characteristic platelet morphology of $VOHPO_4 \cdot 0.5H_2O$ and $VOPO_4 \cdot 2H_2O$ was clearly observed [34].

Due to the significantly low surface areas of these biphasic V promoted MoPO materials, TPR analysis was used to investigate their bulk reducibility, presented in Figures 4c-f. The reduction behaviour of both MoPO-V1 and MoPO-V5 (Figures 4c and 4d) are similar to that of MoPO (Figure 4b), confirming that vanadium in both materials is highly dispersed on the surface (as a separate phase), consistent with our previous characterization. A single but markedly broad reduction peak is present in each profile, and it is attributed to $Mo^{6+} \rightarrow Mo^{4+}$ reduction, however, the increasing V content slightly lowered the peak maximum temperature (Table 1). Taking into consideration the $H_2$ consumption, it is clear that the increasing presence of a vanadium phosphate phase enhances the overall reducibility of the material. The peak temperature of $Mo^{6+} \rightarrow Mo^{4+}$ reduction in the TPR profile of MoPO-V10 (Figure 4e) is displayed at 565 °C, and at 571 °C for MoPO-V20 (Figure 4f). Although the intensity of the main Mo reduction peak is lower for both MoPO-V10 and MoPO-V20 than the other materials, there is also a reduction peak present at a lower temperature of 490 °C, which is assigned to the reduction of $V^{5+} \rightarrow V^{4+}$ [35]. The $H_2$ consumption (Table 1) for both

MoPO-V10 and MoPO-V20 is substantially increased compared to that of MoPO, and for MoPO containing lower quantities of V.

X-ray photoelectron spectroscopy results for MoPO and V promoted catalysts are summarised in Table 1. As expected, MoPO presents a Mo(3d) peak at 233.8 eV, which corresponds to $Mo^{6+}$ species [36,37], and a P(2p) peak at 134.4 eV, attributed to surface $P^{5+}$ [38]. Even though the detection of a VPO phase was not observed using other characterisation techniques for MoPO-V1, XPS results show that a V($2p_{3/2}$) peak at 517.5 eV (0.18 at. %) is attributed to surface $V^{4+}$, which could be associated with the phase, $VOHPO_4 \cdot 0.5H_2O$. The XPS results recorded for MoPO-V5 presents $V^{4+}$ species, which again corresponds to the $VOHPO_4 \cdot 0.5H_2O$ phase observed by XRD and Raman spectroscopy. However, there was also the presence of a second peak at 518.8 eV, which can be assigned to $V^{5+}$ [39]; the ratio of $V^{4+}$:$V^{5+}$ was 70:30 (0.33 at. %). MoPO-V10 also showed both surface $V^{4+}$ and $V^{5+}$ species, but in a 17:83 ratio (1.10 at. %), which again corresponds well with the XRD results where both $VOHPO_4 \cdot 0.5H_2O$ and $VOPO_4 \cdot 2H_2O$ diffraction patterns were observed. MoPO-V20 displayed only surface $V^{5+}$ (4.18 at. %), associated with the $VOPO_4 \cdot 2H_2O$ bulk phase identified by previous characterization.

*3.2 Catalyst Performance for Methanol Oxidation*

Blank reactions carried out in an empty reactor tube only showed very low methanol conversion. Trace conversion was observed initially at 200 °C and conversion increased marginally with temperature, but it was <1% at 500 °C. For the blank reaction the only reaction product was formaldehyde. Selective oxidation of methanol was conducted over the unpromoted and V promoted MoPO catalysts over a temperature range 200 to 480 °C (Table 2). As the reaction temperature was increased, all of the catalysts produced significantly high selectivity towards formaldehyde, even at high conversion of methanol. Figure 5 shows both

methanol conversion and formaldehyde selectivity over the reaction temperature profile, clearly presenting the enhanced activity of V promoted catalysts compared to the unpromoted MoPO catalyst. Table 2 displays the conversions of each catalyst at 200 °C, where a minimal increase in methanol conversion with increasing V content is reported. Although these are subtle enhancements, these can be correlated with the findings from characterization studies. In the case of MoPO-V5, XRD and Raman spectroscopy results confirmed the presence of a biphasic material. Specifically, $VOHPO_4 \cdot 0.5H_2O$ exists in accordance with the main MoPO phase. Catalytic testing of $VOHPO_4 \cdot 0.5H_2O$ during methanol oxidation (under identical reaction conditions) is displayed in Table 3. In comparison with the pure MoPO catalyst (5.3 % conversion), the $VOHPO_4 \cdot 0.5H_2O$ catalyst shows higher conversion at this temperature (8.6 %). Therefore, it is reasonable to suggest that the increase in activity of the biphasic MoPO-V5 catalyst at low temperatures is due to the presence of the vanadium phosphate phase. In correlation with this postulation, the increase in conversion with MoPO-V10 and MoPO-V20 catalysts can be attributed to the presence of $VOPO_4 \cdot 2H_2O$, which achieves 9.6 % conversion at 200 °C (Table 3).

Focusing on product selectivity at these low conversions, each catalyst achieves formaldehyde selectivity above 98 %. However, even at these low conversions, there are subtle selectivity changes towards each product as the V content is increased in the MoPO catalysts. For the unpromoted MoPO catalyst, the only product produced at 200 °C was formaldehyde, which indicates the presence of redox sites on the surface, which are reported as essential for high formaldehyde selectivity [40]. At 200 °C, MoPO-V1 produced 99 % formaldehyde selectivity, but also 1 % methyl formate selectivity, which can be explained *via* the introduction of stronger basic sites and reduced influence from redox sites than in the unpromoted catalyst. Increasing basicity increases the time formaldehyde is adsorbed on the surface, leading to over oxidation to methyl formate [41]. As the vanadium content increases,

there is a further increase of methyl formate selectivity, with MoPO-V20 producing 2.1 %, which suggests that the number of stronger basic/redox sites is increasing with vanadium content.

Comparing catalytic performance at 400 °C, provides a clearer indication of the enhanced activity and selectivity of vanadium promoted catalysts. Methanol conversion of 50.8 % was obtained with MoPO, whereas the incorporation of only 1 mol % V increased the conversion to 71 %, whilst both unpromoted and promoted catalysts achieved 91.4 and 93.2 % formaldehyde selectivity respectively (Table 2). The detection of VPO phases in materials with higher quantities of vanadium, accompanied by XPS data (Table 1), could indicate that a VPO phase is present in MoPO-V1 but is highly dispersed, which could account for its absence using bulk characterization techniques, and could also explain the high activity of this catalyst. MoPO-V5 also produced higher activity than the unpromoted catalyst with 63 % methanol conversion. The increase in conversion compared with MoPO, can be attributed to the presence of $VOHPO_4 \cdot 0.5H_2O$ (Figure 1), which alone gave 84.3 % conversion at 400 °C (Table 3). However, the conversion reached with MoPO-V5 in contrast to MoPO-V1 is lower, which could be due to the lower dispersion of the VPO phase. MoPO-V10 exhibited similar activity to MoPO-V1 with 70 % conversion at the same reaction temperature, which indicates that there is not a simple relationship between vanadium content and activity. Relating to bulk characterization of this sample, we can associate these catalytic features with the presence and dispersion of mixed phases, specifically, $VOHPO_4 \cdot 0.5H_2O$, $VOPO_4 \cdot 2H_2O$ and $(MoO_2)_2P_2O_7$, identified using XRD (Figure 1). Although the use of $VOPO_4 \cdot 2H_2O$ as a catalyst for methanol oxidation at 400 °C is poor in comparison to MoPO (Table 3), its dispersion on the surface of MoPO and/or $VOHPO_4 \cdot 0.5H_2O$ could enhance its catalytic properties. This postulation is exaggerated further with MoPO-V20, which achieves 78 % methanol conversion and 96 % formaldehyde selectivity. XPS surface composition analysis

of this biphasic catalyst (Table 1), displays a dramatic increase in the ratio of V species at the surface, equalling the ratio of Mo species. This indicates a greater dispersion of the VPO phase near the surface, which in turn enhances catalytic activity.

The other by-products produced during the oxidation reaction were DME and CO. Although in relatively low quantities, both MoPO and MoPO-V5 both produce 1 % selectivity to DME, which indicates the presence of acidic as well as basic and redox sites on the surface [42]. The CO selectivity obtained for each V promoted catalyst at high reaction temperatures (480 °C) also reinforces the postulation that the introduction of vanadium phosphate phases heavily influences the catalytic properties of these mixed phase catalysts. The CO selectivity at this temperature obtained with $VOHPO_4 \cdot 0.5H_2O$ is 71 %, in contrast to 10.5 % achieved with MoPO, both at >98 % methanol conversion. XRD and Raman spectroscopy both provided evidence that MoPO-V5 and MoPO-V10 were mixed with $VOHPO_4 \cdot 0.5H_2O$. Considering that both these catalysts obtained the highest CO selectivity (16.4 and 16.2 %, respectively) of all un-promoted and V promoted MoPO catalysts, the influence of the vanadium phosphate phases is clear. No evidence for catalyst deactivation was observed, however, the time-on-stream was relatively short, and to assess the full potential of these catalysts long-term stability studies need to be performed.

Comparing the activity of the most commonly reported catalysts for methanol oxidation to formaldehyde (Table 3), the MoPO and MoPO-V*x* catalysts obtain moderate activity. The commercial ($Fe_2(MoO_4)_3$) catalyst achieves substantially higher activity than that of the MoPO-based catalysts reported here, as total methanol conversion was reached at ~300 °C for $Fe_2(MoO_4)_3$, compared to ~480 °C for MoPO catalysts. However, both types of catalyst demonstrate initial activity at the same temperature (*ca.* 200 °C). Considering the activity of $MoO_3$ in relation to MoPO-V*x* provides a clear indication of the potential of these

molybdenum phosphate catalysts, as at a reaction temperature of 400 °C, there is comparable activity and formaldehyde selectivity.

Analysing the physico-chemical properties of both the unpromoted and the promoted MoPO catalysts, and relating to known catalyst systems, some structure-activity relationships can be determined. It is known that related molybdenum oxide catalysts operate by a Mars-van Krevelen mechanism. The first step of the reaction has been found to be the formation of methoxy groups with a surface cation, by dissociative adsorption of methanol on a dual acid-base site, with a surface oxygen ion providing the basic site [42,43]. The consecutive transformation of the adsorbed methoxy group, not only depends on the acid strength of the site to which it is adsorbed, but also to the nature of neighbouring active centres. It is widely accepted that the rate-limiting step is C-H bond dissociation, and it is determined on the basic or nucleophilic character of oxygen species in close proximity to the adsorbed methoxy group [44-46]. The use of $(MoO_2)_2P_2O_7$ as a methanol oxidation catalyst is reported here for the first time, and much remains to be understood. However, considering some of the structural and chemical similarities to other known effective methanol selective oxidation catalysts, such as $MoO_3$ [47] and $Fe_2(MoO_4)_3$ [48], it is reasonable to assume it operates in a similar manner. For $MoO_3$ and $Fe_2(MoO_4)_3$ it is reported that the main active centre consists of terminal Mo=O, where the oxidation state of Mo plays an important role in the activity of the catalyst, with $Mo^{6+}$ being favourable to $Mo^{5+}$. As the oxidation state of molybdenum in MoPO catalysts is $Mo^{6+}$ and Raman spectra features Mo=O bands at 860, 1001 and 1016 $cm^{-1}$, the active site and mechanism of methanol oxidation may be suggested to be similar to $MoO_3$ and $Fe_2(MoO_4)_3$ catalysts.

Interestingly, in the fresh MoPO catalysts only one surface species of oxygen is present at 531.9 eV (Table 1), which is assigned to that of lattice oxygen, however, in the ex-reactor sample, two species of oxygen are present at 531.9 and 533.1 eV. The presence of the binding

energy peak at 533.1 eV, is attributed to $OH^-$ groups, which suggests that un-reacted methoxy groups are present on the surface [49], or that the surface could be hydroxylated.

## 4. Conclusions

The structural and chemical properties of novel V promoted MoPO catalysts were studied, and their catalytic behaviour investigated for the partial oxidation of methanol to formaldehyde. All the catalysts achieved high formaldehyde selectivity at relatively high methanol conversion, but high reaction temperatures were needed in comparison to the commercial ferric molybdate catalyst. The increasing V content in MoPO catalysts led to a substantial enhancement in activity compared to that of the unpromoted catalyst, whilst obtaining high formaldehyde selectivities. It was observed that varying the V content, formed two additional VPO phases. Addition of low quantities of V led to the formation of $VOHPO_4 \cdot 0.5H_2O$, with higher V content leading to $VOPO_4 \cdot 2H_2O$ formation. The dispersion of these VPO phases at the MoPO surface, were key to the enhanced activity of these mixed phased catalysts. The encouraging activity of MoPO and MoPO/VPO mixed phase catalysts towards methanol oxidation, warrants further investigation.

## Acknowledgements

We would like to thank the EPSRC and Cardiff University for financial support.

## References

[1]: H.R. Gerberich, A.L. Stautzenberger, W.C. Hopkins, Formaldehyde, In: Kirk-Othmer Encyclopaedia of Chemical Technology, John Wiley and Sons, New York, 1980, p. 231-250.

[2]: G. Reuss, W. Disteldorf, O. Grundler, A. Hilt, Formaldehyde, In Ullmann's Encyclopaedia of Industrial Chemistry, VCH Publishers, 1992, p. 619-620.

[3]: J. R. Fair, R.C. Kmetz. Formaldehyde, In Encyclopaedia of Chemical Processing and Design, J.J. McKetta, W.A. Cunningham (Eds.), Marcel Dekker, Inc. 1985, 350-351.

[4]: A.R. Chauvel, P.R. Curty, R. Maux, C. Petitpas, Hydr. Proc. 52 (1973) 179-180.

[5]: A.B. Stiles, T.A. Koch, Oxidation Catalysts: In Catalyst Manufacture, Marcel Dekker, New York, 1995, Chap. 20.

[6]: A. Andreasen, H. Lynggaard, C. Stegelmann, P. Stoltze, Appl. Catal. A. Gen. 289 (2005) 267-273.

[7]: M. Bowker, R. Holroyd, A. Elliot, P. Morrall, A. Alouche, C. Entwistle, A. Toerncrona, Catal. Lett. 83 (3-4) (2002) 165-176.

[8]: G. Reuss, W. Disteldorf, A.O. Gamer, A. Hilt, In Ullmann's Encyclopaedia of Industrial Chemistry, Wiley-VCH, weinheim, 2008, p. 619-652.

[9]: B. Crichton in: Informally Speaking (Newsletter from Perstorp Formox, http://www.perstorpformox.com), spring/summer 2003, p. 12–13.

[10]: Y. Uebou, S. Okada, J. Yamaki, J. Power Sources, 115 (2003) 119-124.

[11]: D. Bhattacharyya, S.K. Bey, M.S, Rao, Appl. Catal. A. Gen. 87 (1992) 29-43.

[12]: M.A. Chaar, D. Patel, H.H. Kung, J. Catal. 109 (1988) 463-467.

[13]: D. S.H. Sam, V. Soenen, J.C. Volta, J. Catal, 123 (1990) 417-435.

[14]: R.H.H. Smits, K. Seshan, J.R.H. Ross, Stud. Surf. Sci. Catal. 72 (1992) 221-229.

[15]: A. Cherrak, R. Hubaut, Y. Barbaux, G. Mairesse, Catal. Lett. 15 (1992) 377-383.

[16]: G. Costentin. L. Savary, J.C. Lavalley, M.M. Borel, A. Grandin, Chem. Mater. 10 (1998) 59-64.

[17]: S. Nianxue, Z. Xuan, J.K. Bartley, S.H. Taylor, D. Chadwick, G.J. Hutchings, Catal. Lett. 106 (2006) 3-4.

[18]: Y.H. Taufiq-Yap, C.K. Goh, G.J. Hutchings, N. Dummer, J.K. Bartley, Catal. Lett. 130 (2009) 327-334.

[19]: P. Bonnet, J.M.M. Millet, C. Leclercq, J.C. Vedrine, J. Catal. 158 (1996) 128-141.

[20]: J.M.M. Millet, J.C. Vedrine, G. Hecquet, Stud. Sci. Catal. 55 (1990) 833-841.

[21]: J. C. Vedrine, Top. Catal. 11/12 (2000) 147-152.

[22]: P. Kierkegaard, Acta. Chem. Scand. 12 (1958) 1701-1703.

[23]: P. Kierkegaard, Ark. Kemi. 19 (1962) 1-14.

[24]: S.E. Lister, A. Soleihavoup, R. Withers, P. Hodgkinson, J. Evans, Inorg. Chem. 49 (2010) 2290-2301.

[25] D. Boudlich, L. Bih, M. E. H. Archidi, M. Haddad, A. Yacoubi, A. Nadiri, B. Elouadi. J. Am. Ceram. Soc., 85 (2002) 623-630.

[26]: N. Duvauchelle, E. Kesteman, F. Oudet, E. Bordes, J. Solid State Chem. 137 (1998) 311-324.

[27]: X. Zhang, H-L. Wan, W-Z. Weng, X-D. Yi, Appl. Surf. Sci. 220 (2003) 117-124.

[28]: L. O'Mahony, J. Henry, D. Sutton, T. Curtin, B.K. Hodnett, Appl. Catal. A: Gen. 253 (2003) 409–416.

[29]: L. O'Mahony, D. Sutton, B.K. Hodnett, Catal.Today 9/92 (2004) 185–189.

[30]: L. O'Mahony, T. Curtin, J. Henry, D. Zemlyanov, M. Mihov, B.K. Hodnett. Appl. Catal. A: Gen. 285 (2005) 36–42.

[31]: Y.C. Wong, Y.H, T-Yap, Asian J. Chem. 23 (2011) 3853-3858.

[32]: V.V. Guliants, J.B. Benziger, S. Sundaresan, I.E. Wachs, J.-M. Jehng, J.E. Roberts, Catal. Today 28 (1995) 275-295.

[33]: J.K. Bartley, C.J. Kiely, R.P.K. Wells, G.J. Hutchings, Catalysis Letters, 72 (2001) 99-105.

[34]: L. Griesel, J.K. Bartley, R.P.K. Wells, G.J. Hutchings, J. Mol. Catal. A: Chem. 220

(2004) 113-119.

[35]: P. Concepcion, J.M.L. Nieto, J.P-Pariente, J. Mol. Catal. A: Chem. 99 (1995) 173-182.

[36]: L.E. Firment, A. Faretti, Surf. Sci. 129 (1983) 155-176.

[37]: T.H. Fleisch, G.J. Mains, J. Chem. Phys. 76 (1982) 780-786.

[38]: A. Medina, J.L. Solis, J. Rodriguez, W. Estrada, Sol. Energy Mater. Sol. Cells, 80 (2003) 473-481.

[39]: M.P. Casaletto, S. Kaciulis, L. Lisi, G. Mattogno, A. Mezzi, P. Patrono, G. Ruoppolo, Appl. Catal. A: Gen. 218 (2001) 129-137.

[40]: J.M. Tatibouet, Appl. Catal. A: Gen. 148 (1997) 213-252.

[41] G. Busca, J. Mol. Catal., 50 (1989) 241-249.

[42]: M. Ai, J. Catal. 54 (1978) 426-435.

[43]: N. Pernicone, F. Lazzerin, G. Liberti, G. Lanzavecchia, J. Catal. 14 (1969) 293-302.

[44]: T.J. Yang, J.H. Lunsford, J. Catal., 103 (1987) 55-64.

[45]: C.J. Machiels, A.W. Sleight, J. Catal. 76 (1982) 238-239.

[46]: W.E. Farneth, F. Ohuchi, R.H. Staley, U. Chowdhry, A.W. Sleight, J. Phys. Chem. 89 (1985) 2493-2497.

[47]: J.M. Jehng, H. Hu, X. Gao, I.E. Wachs. Catal. Today. 28 (1996) 335-350.

[48]: M. Bowker, R. Holroyd, M. House, R. Bracey, C. Bamroobgwongdee, M. Shannon, A. Carley, Top. Catal. 48 (2008) 158-165.

[49]: J. Haber, E. Lalik, Catal. Today, 33 (1997) 119-137.

.

## Figure captions

**Figure 1:** Powder X-ray diffraction patterns: a). MoHPO; b). MoPO; c). MoPO-V1; d). MoPO-V5; e). MoPO-V10; f). MoPO-V20.

**Figure 2:** Laser Raman spectra: a). MoHPO; b). MoPO; c). MoPO-V1; d). MoPO-V5; e). MoPO-V10; f). MoPO-V20.

**Figure 3:** Scanning electron microscopy images: a). MoHPO; b). MoPO; c). MoPO-V1; d). MoPO-V5; e). MoPO-V10; f). MoPO-V20.

**Figure 4:** Temperature programmed hydrogen reduction profiles: a). MoHPO; b). MoPO; c). MoPO-V1; d). MoPO-V5; e). MoPO-V10; f). MoPO-V20.

**Figure 5:** Performance of catalysts for methanol oxidation; A: Methanol conversion, B: Formaldehyde selectivity: —□— = MoPO: —▲— = MoPO-V1: —◆— = MoPO-V5: —■— = MoPO-V10: —●— = MoPO-V20

**Table 1:** Physico-chemical properties of unpromoted and V promoted MoPO materials.

| Material | $S_{BET}$ ($m^2$ $g^{-1}$) | TPR | | XPS Binding Energy (eV) | | | XPS metal surface concentration (At. %) | |
|---|---|---|---|---|---|---|---|---|
| | | Reduction peak Temperatures (°C) | $H_2$ consumption ($\mu$mol $g^{-1}$) | Mo(3d) | V($2p_{3/2}$) | O(1s) | Mo | V |
| **MoHPO** | 1 | 557 | 1422 | 233.6 | - | 513.9 | 9.2 | - |
| **MoPO** | 1 | 579 | 1646 | 233.8 | - | 531.9 | 7.5 | - |
| **MoPO-V1** | 1 | 571 | 1693 | 233.6 | 517.5 | 531.7 | 9.2 | 0.2 |
| **MoPO-V5** | 1 | 571 | 1746 | 233.6 | 517.2, 518.8 (70:30) | 531.8 | 8.9 | 0.3 |
| **MoPO-V10** | 1.5 | 490, 565 | 1806 | 233.8 | 517.2, 518.8 (17:83) | 531.9 | 8.4 | 1.1 |
| **MoPO-V20** | 3 | 490, 571 | 1923 | 233.6 | 518.7 | 531.6 | 4.2 | 4.2 |

**Table 2:** Catalytic performance of unpromoted and V promoted MoPO catalysts in methanol selective oxidation.

| Catalyst | Temperature (°C) | MeOH Conv. (%) | Selectivities (%) | | | | | FA Yield (mol %)[a] |
|---|---|---|---|---|---|---|---|---|
| | | | DME | MF | FA | CO | $CO_2$ | |
| **MoPO** | 200 | 5.3 | - | - | 100 | - | - | 5.3 |
| | 400 | 50.8 | 1 | - | 91.4 | 7.6 | - | 46.4 |
| | 480 | 95.8 | - | - | 89.5 | 10.5 | - | 85.7 |
| **MoPO-V1** | 200 | 5.4 | - | 1 | 99 | - | - | 5.3 |
| | 400 | 71.4 | - | - | 93.2 | 6.8 | - | 66.5 |
| | 480 | 99.5 | - | - | 88 | 10.9 | 1.1 | 87.6 |
| **MoPO-V5** | 200 | 7.7 | - | 1.4 | 99.6 | - | - | 7.7 |
| | 400 | 62.5 | 1 | - | 92.8 | 7.2 | - | 58.0 |
| | 480 | 96.4 | - | - | 81.9 | 16.4 | 1.7 | 78.9 |
| **MoPO-V10** | 200 | 8 | - | 1.6 | 99.4 | - | - | 7.9 |
| | 400 | 70 | - | - | 93.8 | 6.2 | - | 65.7 |
| | 480 | 99.5 | - | - | 81.7 | 16.2 | 2.1 | 81.3 |
| **MoPO-V20** | 200 | 6.4 | - | 2.1 | 97.9 | - | - | 6.3 |
| | 400 | 77.6 | - | - | 95.8 | 7.6 | - | 74.3 |
| | 480 | 99.4 | - | - | 82.5 | 16 | 1.5 | 82.0 |

*a*: Formaldehyde per pass yield (mol %).

**Table 3:** Catalytic performance of alternative selective methanol oxidation catalysts.

| Catalyst | Temperature (°C) | MeOH Conv. (%) | Selectivities (%) | | | | | FA Yield (mol %) |
|---|---|---|---|---|---|---|---|---|
| | | | DME | MF | FA | CO | $CO_2$ | |
| $Fe_2(MoO_4)_3$ | 200 | 6.2 | - | - | 100 | - | - | 6.2 |
| | 250 | 50.6 | 1.8 | - | 95.5 | 2.7 | - | 48.3 |
| | 300 | 99.3 | - | | 92.2 | 7.8 | - | 91.5 |
| $MoO_3$ | 200 | 1.5 | 100 | - | - | - | - | - |
| | 400 | 85 | - | 2.6 | 91.3 | 4.7 | 1.4 | 77.6 |
| | 450 | 99.8 | - | - | 86 | 9.8 | 4.2 | 85.8 |
| $VOHPO_4 \cdot 0.5H_2O$ | 200 | 8.6 | - | - | 100 | - | - | 8.6 |
| | 400 | 84.3 | 1.2 | - | 74.8 | 22.8 | 1.2 | 63.1 |
| | 480 | 95.7 | - | - | 29.0 | 71.0 | - | 27.8 |
| $VOPO_4 \cdot 2H_2O$ | 200 | 9.6 | - | - | 100 | - | - | 9.6 |
| | 400 | 40.6 | 1.4 | - | 98.6 | - | - | 40.0 |
| | 480 | 99.5 | - | - | 78.4 | 13.3 | 8.3 | 78 |

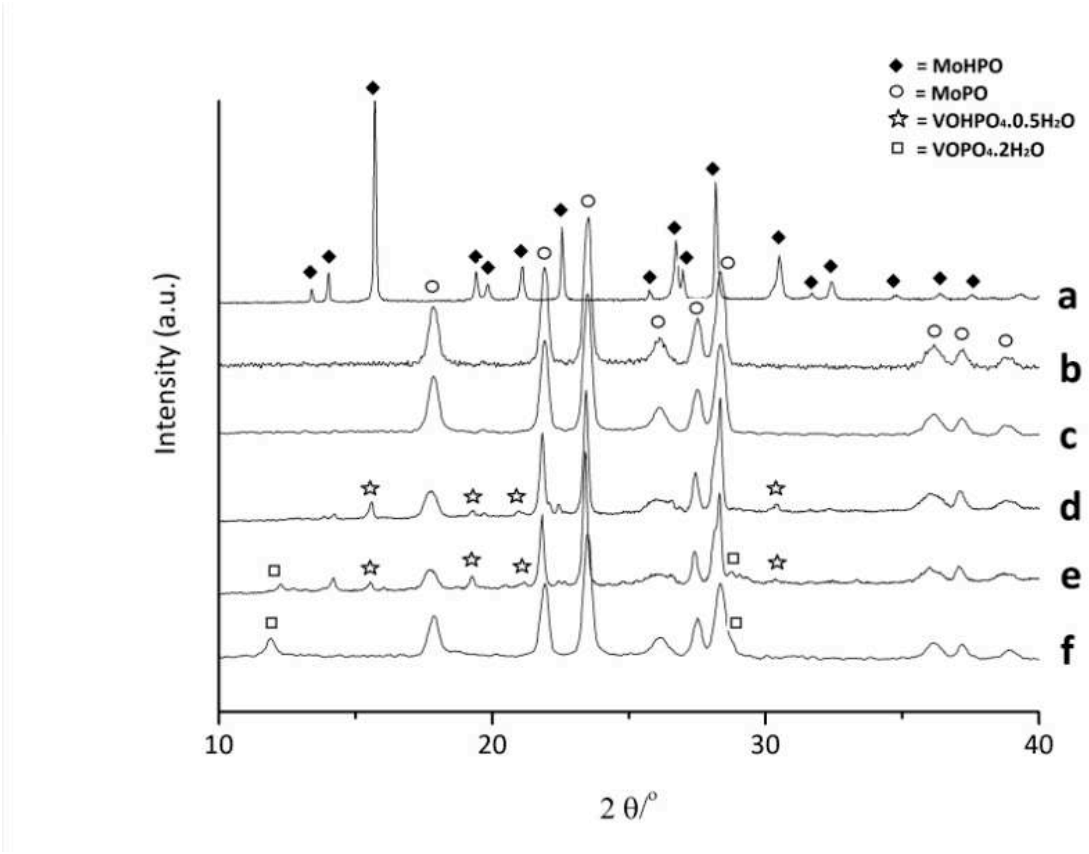
◆ = MoHPO
○ = MoPO
☆ = VOHPO4.0.5H2O
□ = VOPO4.2H2O
Intensity (a.u.)
a
b
c
d
e
f
10
20
30
40
2 θ/°

**Fig. 1**

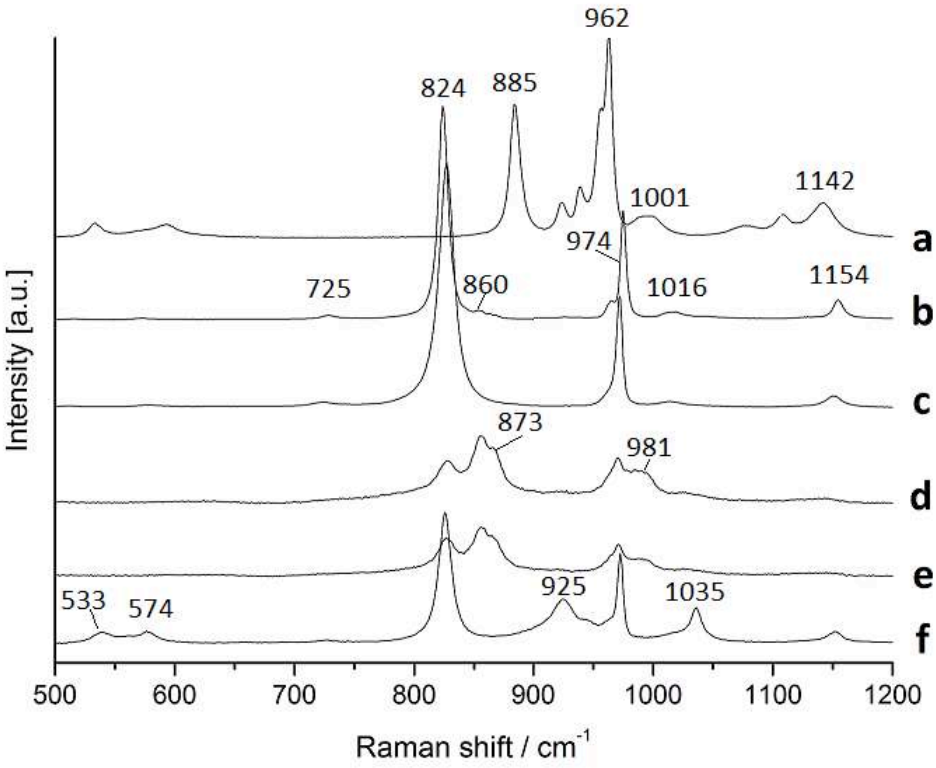
962
824
885
1001
1142
974
725
860
1016
1154
a
b
c
873
981
d
e
925
1035
533
574
f
Intensity [a.u.]
500
600
700
800
900
1000
1100
1200
Raman shift / cm-1

**Fig. 2**

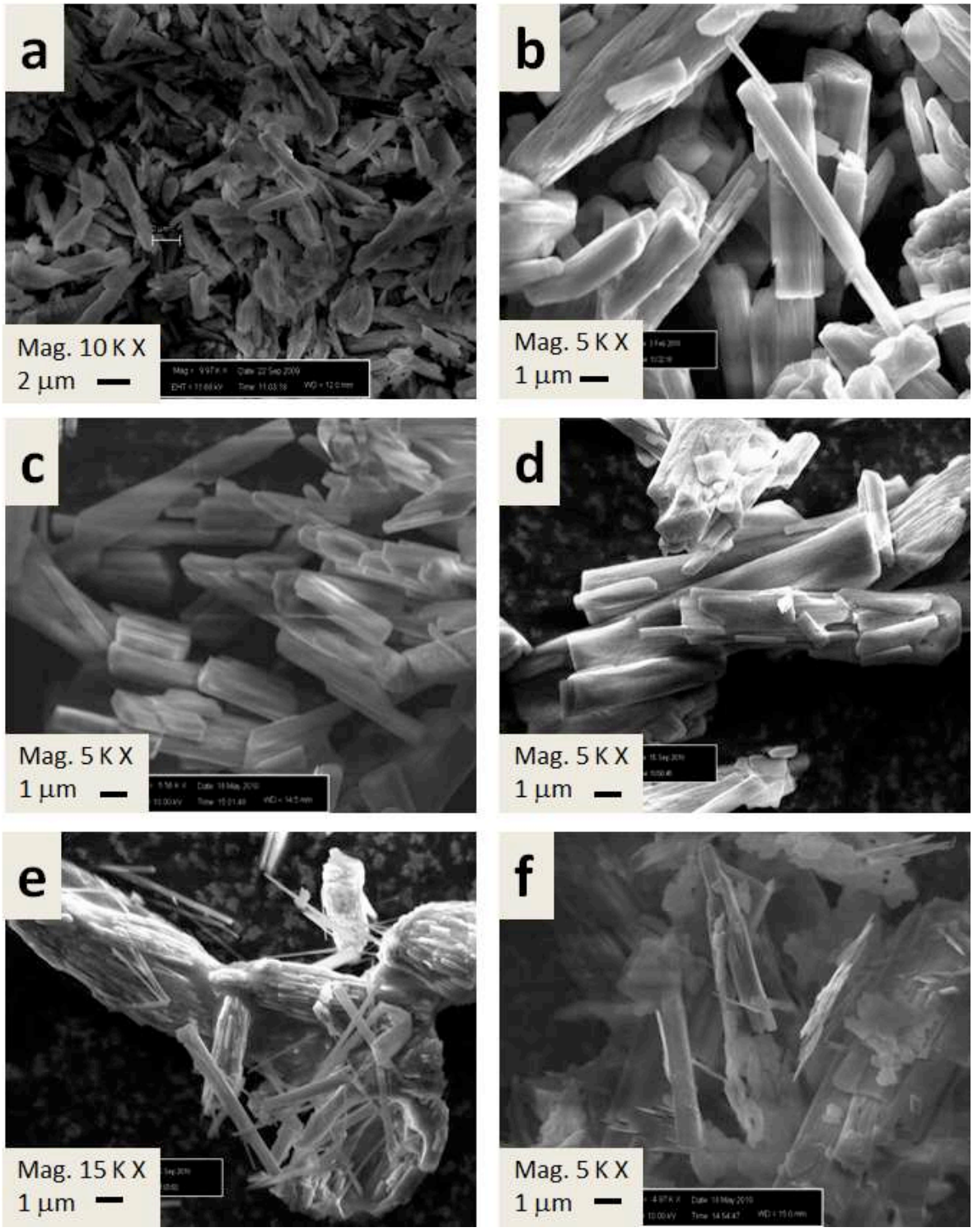
a
Mag. 10 K X
2 µm
b
Mag. 5 K X
1 µm
c
Mag. 5 K X
1 µm
d
Mag. 5 K X
1 µm
e
Mag. 15 K X
1 µm
f
Mag. 5 K X
1 µm

**Fig. 3**

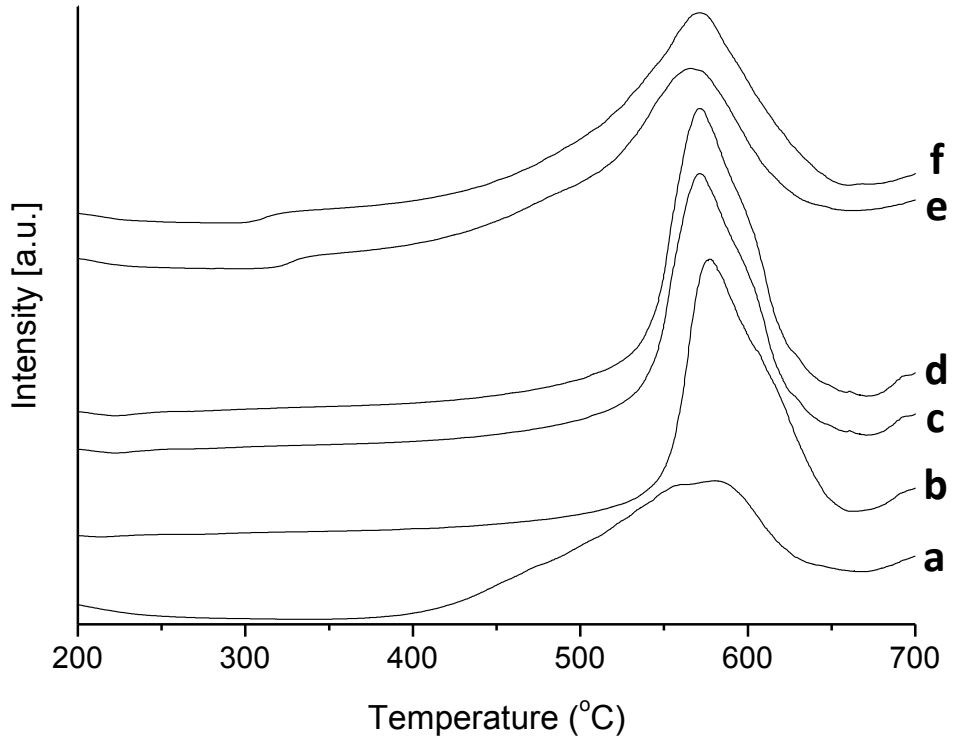


**Fig. 4**

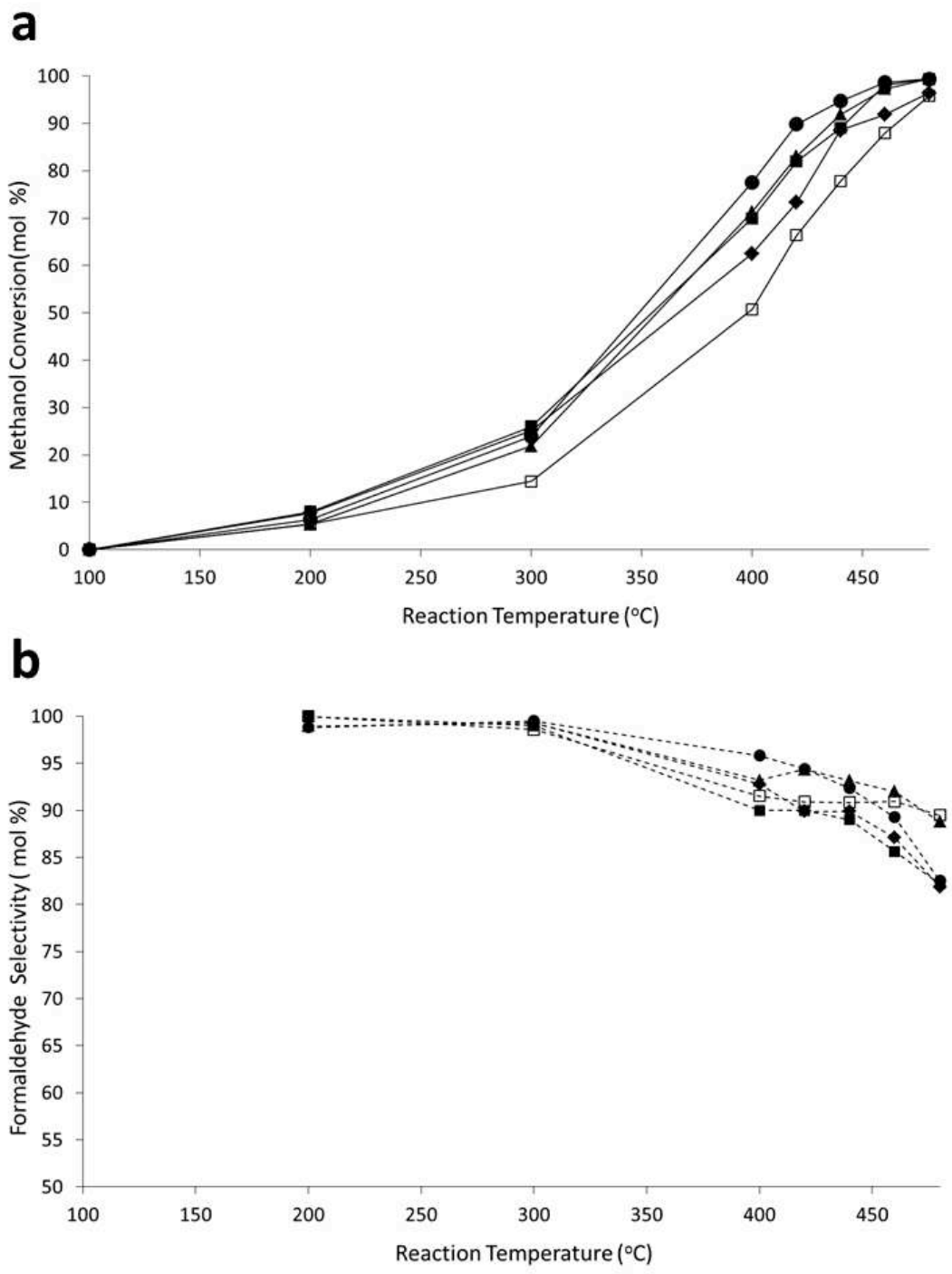
a
Methanol Conversion(mol %)
Reaction Temperature (°C)
b
Formaldehyde Selectivity ( mol %)
Reaction Temperature (°C)

**Fig. 5**